Inverse spin Hall effect in the semiconductor (Ga,Mn)As at room temperature

J. B. S. Mendes,[1,*] S. L. A. Mello,[1] O. Alves Santos,[2] R. O. Cunha,[3] R. L. Rodríguez-Suárez,[4] A. Azevedo,[2] and S. M. Rezende[2]

[1]*Departamento de Física, Universidade Federal de Viçosa, 36570-900 Viçosa, Minas Gerais, Brazil*
[2]*Departamento de Física, Universidade Federal de Pernambuco, 50670-901 Recife, Pernambuco, Brazil*
[3]*Centro Interdisciplinar de Ciências da Natureza, Universidade Federal da Integração Latino-Americana, 85867-970 Foz do Iguaçu, Paraná, Brazil*
[4]*Facultad de Física, Pontifícia Universidad Católica de Chile, Casilla 306, Santiago, Chile*

(Received 8 March 2017; revised manuscript received 9 May 2017; published 9 June 2017)

We report experiments demonstrating that a spin current can be converted into a charge current in a film of the paramagnetic semiconductor (Ga,Mn)As at room temperature by means of the inverse spin Hall effect. The spin currents are generated in a thin layer of permalloy (Py) by two different processes: spin-pumping effect (SPE) and spin Seebeck effect (SSE). In the first, we use microwave-driven ferromagnetic resonance of the Py film to generate a SPE spin current that is injected into the (Ga,Mn)As film either in direct contact with Py or through a thin layer of insulating antiferromagnetic NiO. In the second, we use the SSE in the longitudinal configuration in Py with no contamination by the Nernst effect made possible with the use of a thin layer of NiO between the Py and (Ga,Mn)As layers. The results of the two measurements are consistent with each other, and from them, we obtain a spin Hall angle for (Ga,Mn)As at room temperature of $\theta_{SH} = (1.5 \pm 0.5)\times 10^{-3}$, which is one order of magnitude larger than the values reported for p-Si and n-Ge at room temperature.

DOI: 10.1103/PhysRevB.95.214405

I. INTRODUCTION

The spin Hall effect (SHE) and its Onsager reciprocal, the inverse SHE (ISHE), play a very important role in spintronics because they make possible the conversion of charge currents into spin currents and vice versa [1–5]. Since the SHEs rely on the spin-orbit interaction, most studies of the spin-to-charge conversion have been conducted in metallic films with heavy elements, such as paramagnetic Pt, Pd, and Ta, ferromagnetic (FM) Py, and anti-FM materials, such as IrMn and PtMn [3–21]. The spin-to-charge current conversion is an especially important phenomenon in semiconductors because it makes possible the integration of spintronics with electronics. One difficulty here is that, in the most important semiconductors, namely silicon (Si) and gallium arsenide (GaAs), the spin-orbit coupling is small, and so are the SHEs. Nevertheless, the first observation of the SHE was made in GaAs at low temperatures with optical detection techniques [22], but very few studies on spin-to-charge current conversion and spin transport in semiconductors have been reported in the literature [23–28].

Since its FM properties were revealed by Ohno *et al.* [29] and Ohno [30], the semiconductor $Ga_{1-x}Mn_xAs$ has attracted considerable attention of experimentalists and theoreticians because one can add to the semiconducting properties a new degree of freedom associated with the spin of the carriers [31–37]. Recently, (Ga,Mn)As gained renewed attention for demonstrating spintronic phenomena, such as the spin Seebeck effect (SSE) [38], spin-pumping effect (SPE) [39], and magnonic charge pumping (MCP) [40]. However, all the reported experiments were done in the FM phase of (Ga,Mn)As at low temperatures (<50 K), which represents a strong limitation for practical applications.

In this paper, we report the observation of spin-to-charge current conversion by means of the ISHE in the paramagnetic phase of (Ga,Mn)As at room temperature. The spin currents are generated by two different schemes: microwave driven SPE and the SSE. In Sec. II, we describe the sample preparation and characterization with magnetotransport techniques. In Sec. III, we present experimental results with FM resonance (FMR) driven SPE, from which we obtain an initial measurement of the spin Hall angle of (Ga,Mn)As. In Sec. IV, we present measurements with the SSE, which are used to confirm the results obtained with SPE. Finally, in Sec. V, we discuss the results and compare them to those obtained in other semiconductor materials.

II. SAMPLE PREPARATION AND CHARACTERIZATION

The experiments were carried out with two sample structures, one consisting of a simple bilayer of (Ga,Mn)As with $Ni_{81}Fe_{19}$ [permalloy (Py)] and the other consisting of a trilayer in which a NiO layer is grown between (Ga,Mn)As and Py. In all of them, we have used a commercial 0.3 mm thick semi-insulating (001) GaAs substrate onto which first a 100 nm thick GaAs buffer layer was grown at a temperature of ∼590 °C by molecular beam epitaxy (MBE). The substrate was then cooled down to ∼265 °C for a low-temperature MBE (LT-MBE) growth of a 3 nm thick GaAs buffer, followed by a 46 or 92 nm thick $Ga_{1-x}Mn_xAs$ layer with nominal Mn concentration $x = 0.05$, according to the method described in Refs. [29,41]. The GaAs/(Ga,Mn)As wafer was then cleaved into pieces with lateral dimensions 1.5×4.0 mm for the fabrication of the samples used in this investigation. For the simple bilayer structure, a layer of the metallic ferromagnet Py with thickness 12 nm and length 2.1 mm was deposited by dc magnetron sputtering on the central part of the (Ga,Mn)As layer. Finally, two indium electrodes were attached to the ends at a distance of 3.5 mm for measuring the induced voltages. For the trilayer

*Corresponding author: joaquim.mendes@ufv.br

  ©2017 American Physical Society

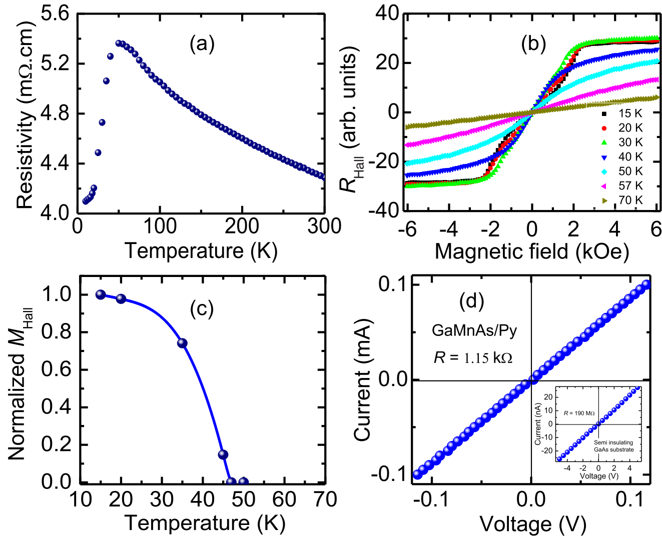

FIG. 1. Transport measurements in 46 nm thick $Ga_{0.95}Mn_{0.05}As$ layer. (a) Temperature dependence of the resistivity. (b) Magnetic field dependence of the Hall resistance at several temperatures as indicated. (c) Temperature dependence of the normalized Hall magnetization obtained from the data in (b). $I \times V$ curve measured at room temperature. The inset shows $I \times V$ curve for the GaAs substrate.

structure, a NiO layer was deposited by rf magnetron sputtering at 160 °C onto the (Ga,Mn)As, and then the Py layer was deposited by dc magnetron sputtering.

Before deposition of the Py or NiO layers, samples of GaAs/(Ga,Mn)As were characterized by magnetotransport measurements. Figure 1(a) shows the temperature dependence of the resistivity ρ of the (Ga,Mn)As (46 nm) layer. As characteristics of (Ga,Mn)As systems, one can observe two distinct behaviors for the resistivity $\rho(T)$ curve: a semiconducting one, characterized by $d\rho/dT < 0$, from room temperature down to $T_\rho \sim 47$ K [where T_ρ denotes the peak temperature of the $\rho(T)$ curve]; and a metallic one, $d\rho/dT > 0$, for temperatures below T_ρ. As is well known [35], $T_\rho \approx T_C$, the critical temperature of the paramagnetic-to-FM transition in (Ga,Mn)As. This behavior is evidenced by the magnetotransport measurements in Fig. 1(b), showing the magnetic field dependence of the Hall resistance for several temperatures. For $T > 47$ K, the Hall resistance varies linearly with field, as in an ordinary semiconductor, while for $T < 47$ K, one can observe a clear tendency to saturation of the Hall resistance as the magnetic field intensity increases above 2 kOe. Such a saturation of the Hall resistance is due to a contribution of the anomalous Hall effect and reveals that the (Ga,Mn)As film is in the FM phase. From the Hall resistance measurements, one can obtain the temperature dependence of the Hall magnetization M_{Hall} using Arrott plots showing $(\rho_{\text{Hall}}/\rho)^2$ versus $H/(\rho_{\text{Hall}}/\rho)$ [42]. Figure 1(c) shows the temperature dependence of M_{Hall}, normalized by its value at $T = 15$ K, for the $Ga_{0.95}Mn_{0.05}As$ sample used in this paper. All other measurements presented in this paper were carried out at room temperature, where $Ga_{0.95}Mn_{0.05}As$ is in the paramagnetic phase. Figure 1(d) shows the measured linear $I \times V$ characteristics, indicating Ohmic contacts with a resistance $R_S = 1.15\,\text{k}\Omega$. The inset shows the $I \times V$ curve of the GaAs substrate, measured before deposition of the (Ga,Mn)As layer, indicating a resistance of 190 MΩ, showing that the (Ga,Mn)As/Py bilayer is effectively isolated from the substrate for charge and spin transport.

III. SPIN-PUMPING EXPERIMENTS

For the FMR and spin-pumping experiments, the sample was mounted on the tip of a polyvinyl chloride (PVC) rod and inserted through a hole drilled in the center of the back wall of a rectangular microwave cavity operating in the TE_{102} mode, at a frequency of 8.55 GHz with a Q factor of 2000. The sample is placed in the plane of the back wall, in a position of maximum rf magnetic field and minimum rf electric field to avoid the generation of galvanic effects driven by the electric field. With this arrangement, the static magnetic field H and the microwave field h_{rf} are in the film plane and kept perpendicular to each other as the sample is rotated for the measurements of the angular dependence of the FMR spectra and the dc voltage induced by the magnetization precession. Field scan spectra of the derivative of the microwave absorption dP/dH are obtained by modulating the field at 1.2 kHz and using lock-in detection. All FMR and voltage measurements were made at room temperature.

Figure 2(a) shows a schematic illustration of the (Ga,Mn)As (46 nm)/Py (12 nm) bilayer sample used in the initial experiments. Figure 2(b) shows the FMR absorption spectrum of the Py layer in contact with the (Ga,Mn)As film measured with microwave power of 16 mW. The FMR line has the shape of a Lorentzian derivative with peak-to-peak linewidth of 37 Oe, corresponding to a half-width at half-maximum (HWHM) linewidth of $\Delta H = 32$ Oe. An identical Py layer deposited on a SiO substrate has linewidth $\Delta H_{\text{Py}} = 27$ Oe, showing that the contact of the (Ga,Mn)As layer produces an additional damping due to the spin-pumping process [43,44], similar to what is observed in Pt/Py bilayers [8,10]. The magnetocrystalline anisotropy of Py, measured by the change in the field for resonance H_R as the sample is rotated in the plane, is 5 Oe, which is very small compared to H_R at microwave frequencies. In this case, the FMR frequency given by the Kittel equation can be written as $f = \gamma\, H_R^{1/2}(H_R + 4\pi M_{\text{eff}})^{1/2}$, where γ is the gyromagnetic ratio, $4\pi M_{\text{eff}} = 4\pi M_0 - K_S/t_{\text{Py}}$ is the effective magnetization, which is smaller than the saturation magnetization $4\pi M_0$ due to the effect of the perpendicular anisotropy in thin films expressed by the term K_S/t_{Py}, where K_S is the surface anisotropy constant and t_{Py} the film thickness. Using the measured $H_R = 0.822$ kOe and $\gamma = 2.94$ GHz/kOe, corresponding to a g factor for Py of 2.1, we obtain $4\pi M_{\text{eff}} = 9.47$ kG. Considering $4\pi M_0 = 11.5$ kG and $t_{\text{Py}} = 12$ nm, this leads to a surface anisotropy constant $K_S = 2.4\times10^{-3}$ Oe.cm, a value similar to the one obtained in Ref. [10] for Py/Pt.

Figure 2(c) shows the field scan dc voltage measured directly with a nanovoltmeter connected by copper wires to the electrodes with the polarity shown in Fig. 2(a), for a microwave power of 16 mW, for three angles of the in-plane magnetic field. For $\phi = 0$, the voltage line shape is the superposition of symmetric and antisymmetric components, changes sign with inversion of the field, and vanishes for the field along the sample strip $\phi = 90°$. The contributions to the dc voltage arise from several sources. The most important and

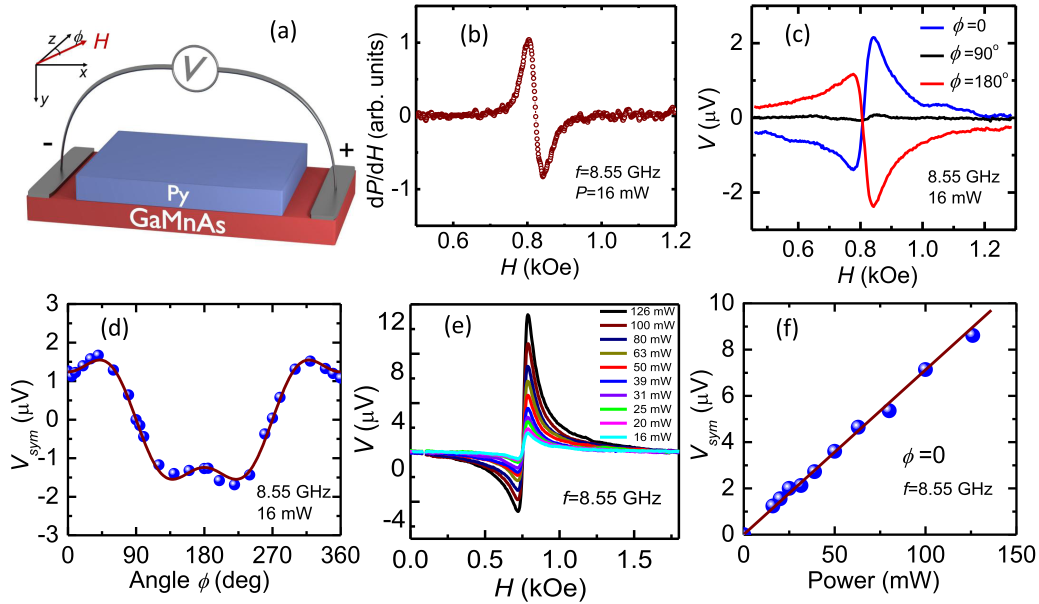

FIG. 2. (a) Sketch of the bilayer sample (Ga,Mn)As (46 nm)/Py (12 nm) and coordinate system. The 0.3 mm thick GaAs substrate is not shown. (b) FMR absorption derivative versus magnetic field H measured at 8.55 GHz and microwave power of 16 mW. (c) Voltage measured between the electrodes for three angles of the in-plane field, with the same microwave frequency and power as in (b). (d) Angular dependence of the symmetric (peak) component of the voltage line. The experimental data are represented by the symbols and the theoretical fit by the solid curve. (e) Voltages measured at several microwave power levels as indicated. (f) Power dependence of the measured symmetric (peak) component of the voltage at $\phi = 0$.

the one of interest here is the conversion of the spin current produced by spin pumping into charge current by the ISHE in the semiconductor (S) layer. As is well known [3–10], in an FM layer under FMR, the precessing magnetization generates a spin current density at the FM/S interface ($y = 0$) given by

$$J_S(0) = \frac{\hbar\,\omega\,p\,g_{\mathrm{eff}}^{\uparrow\downarrow}}{4\pi}\left(\frac{h_{\mathrm{rf}}}{\Delta H}\right)^2 L(H - H_R), \tag{1}$$

where $g_{\mathrm{eff}}^{\uparrow\downarrow}$ is the real part of the effective spin mixing conductance at the interface that takes into account the spin-pumped and backflow spin currents [3–10,43,44], ω and h_{rf} are, respectively, the frequency and amplitude of the driving microwave magnetic field, p is the precession ellipticity, and $L(H - H_R) = \Delta H^2/[(H - H_R)^2 + \Delta H^2]$ is the normalized Lorentzian function. The spin current that flows through the FM/S interface produces a pure spin current in the S layer, formed by charge carriers with opposite spins moving in opposite directions and given by the gradient of the spin accumulation [43,44]. This diffuses into the S layer with a characteristic length given by the spin-flip diffusion length λ_S, which is on the order of several tens of nanometers in semiconductors and only a few nanometers in metals with large spin-orbit scattering. Then a fraction of the charge carriers undergoes spin-orbit scattering generating a transverse charge motion with current density $\vec{J}_C$ given by $\vec{J}_C = \theta_{\mathrm{SH}}(2e/\hbar)\,\vec{J}_S\times\hat{\sigma}$, where θ_{SH} is the spin Hall angle and $\hat{\sigma}$ is the spin polarization. This produces a dc voltage along the length L of the FM layer that is measured at the contacts placed at the ends of the S layer. Integration of the charge current density along x and y gives for the spin-pumping voltage [3]

$$V_{\mathrm{SP}} = R_{\parallel}\, w\lambda_S \frac{2e}{\hbar}\theta_{\mathrm{SH}} \tanh\left(\frac{t_S}{2\lambda_S}\right) J_S \cos\phi_M, \tag{2}$$

where J_S is the spin current density at the interface, t_S and w are the thickness and width of the S layer, $R_{\parallel}$ is the parallel resistance of the FM and S layers, and ϕ_M is the angle of the static magnetization with the direction of the measured charge current. For the case of Py, that has negligible in-plane anisotropy, the magnetization is aligned with the applied magnetic field H so that $\phi_M = \phi$, the field angle with the z axis as shown in Fig. 2(a).

The voltage $V(H)$ between the electrodes has, in addition to the spin-pumping-ISHE component with a symmetric Lorentzian line shape, as in Eq. (1), other contributions of classical origin with symmetric and antisymmetric components. The most important ones are the galvanic effect, or spin rectification, generated in the Py layer and the anomalous Hall effect in the (Ga,Mn)As layer [3–10,23–25]. Both have field and angle dependencies given by

$$V_{\mathrm{CL}}(H,\phi) = \left[V_{\mathrm{CL}}^{\mathrm{sym}}\, L(H - H_R) + V_{\mathrm{CL}}^{\mathrm{asym}}\, D(H - H_R)\right] \sin 2\phi \sin\phi, \tag{3}$$

where $D(H - H_R)$ is an antisymmetric Lorentzian derivative function, while $V_{\mathrm{CL}}^{\mathrm{sym}}$ and $V_{\mathrm{CL}}^{\mathrm{asym}}$ denote the amplitudes of the symmetric and antisymmetric components of the classical contributions to the line shape. Note that, since $L(0) = 1$, $V_{\mathrm{CL}}^{\mathrm{sym}}$ represents the peak value of the symmetric component. Thus, the total voltage measured between the electrodes is given by

$$V(H,\phi) = V_Q^{\mathrm{peak}}\, L(H - H_R)\cos\phi + \left[V_{\mathrm{CL}}^{\mathrm{sym}}\, L(H - H_R) + V_{\mathrm{CL}}^{\mathrm{asym}}\, D(H - H_R)\right] \sin 2\phi\ \sin\phi, \tag{4}$$

where $V_Q^{\rm peak}$ is the peak value of the symmetric contribution to the voltage of quantum origin, of which the spin-pumping-ISHE, given by Eqs. (1) and (2), is one of them. The standard method [3–10] to separate the various contributions consists of measuring the dependence of the voltage line shape $V(H)$ on the angle ϕ and fitting the measured lines with a superposition of two functions in the form $V(H) = V_{\rm sym}\,L(H - H_R) + V_{\rm asym}\,D(H - H_R)$, where $V_{\rm sym}$ and $V_{\rm asym}$ denote, respectively, the amplitudes of the symmetric and antisymmetric components. Figure 2(d) shows the measured angle dependence of the symmetric component only, which is the one of interest here, and a solid curve representing the fit obtained with $V_{\rm sym}(\phi) = V_{\rm SP}^{\rm peak}\cos\phi + V_{\rm CL}^{\rm sym}\sin 2\phi\,\sin\phi$, where $V_Q^{\rm peak} = 1.24\ \mu$V and $V_{\rm CL}^{\rm sym} = 0.94\ \mu$V. Figure 2(e) shows voltage line shapes measured at several power levels, and Fig. 2(f) shows the variation with power of the symmetric component at $\phi = 0$, which is $V_Q^{\rm peak}$, obtained with the fitting procedure. The linear dependence of $V_Q^{\rm peak}$ with power is the behavior expected for the spin-pumping voltage, as given by Eqs. (1) and (2).

From the results above, we can calculate the apparent spin Hall angle of (Ga,Mn)As using Eqs. (1) and (2). Initially, we need the value of the real part of the spin mixing conductance of the (Ga,Mn)As/Py interface, which can be inferred from the broadening of the FMR linewidth due to the spin-pumping process using $g_{\rm eff}^{\uparrow\downarrow} = (4\pi M_0\, t_{\rm Py}/\hbar\,\omega)(\Delta H - \Delta H_{\rm Py})$ [3–5,8,43–45]. With $4\pi M_0 = 11.5$ kG, $t_{\rm Py} = 12$ nm, $\omega/2\pi = 8.55$ GHz, we find that the additional linewidth of 5 Oe measured in Py due to the contact with the (Ga,Mn)As layer corresponds to $g_{\rm eff}^{\uparrow\downarrow} = 1.02\times10^{15}\ {\rm cm}^{-2}$, a value similar to the one for Py/Pt interfaces [3–10]. The amplitude of the microwave field in Eq. (1), in oersteds, is related to the incident power P_i, in watts, by $h_{\rm rf} = 1.509\,(P_i)^{1/2}$, calculated for a microwave cavity made with a shorted standard X-band rectangular waveguide, operating in the TE_{102} mode with Q factor of 2000, at a frequency of 8.55 GHz. Using these values, we obtain for $P_i = 16$ mW, $H = H_R$, the spin current density at the interface produced by the FMR spin pumping $J_S = 4.89\times10^{-8}\ {\rm erg/cm}^2$. Using this value in Eq. (2), considering that the shunt resistance is approximately the one of the Py layer, $R_\parallel \approx 72.5\ \Omega$, $w = 0.15$ cm, $t_S = 46$ nm, and $\lambda_S = 55$ nm (this will be explained later), we obtain for the SPE-ISHE voltage $V_{\rm SPE} = 352\,\theta_{\rm SH}\ \mu$V. If we assume that the measured voltage $V_Q^{\rm peak} = 1.24\ \mu$V is entirely due to the ISHE in (Ga,Mn)As, this result gives for the spin Hall angle $\theta_{\rm SH} = 3.52\times10^{-3}$. However, at this point, it is not possible to attribute the value of $V_Q^{\rm peak}$ entirely to the spin-pumping-ISHE process. As recently discovered [46], a single layer of metallic Py under FMR generates a voltage signal due to the MCP effect [40] that has the same angle and power dependencies of the spin-pumping-ISHE. Hence, since the Py and (Ga,Mn)As layers are in electric contact, the measured $V_Q^{\rm peak}$ may have contributions from spin pumping and from MCP.

In order to measure the spin-pumping-ISHE voltage without the contamination of the MCP, we have made additional FMR-spin-pumping voltage measurements by inserting a thin NiO layer between the (Ga,Mn)As and the Py layers, as shown schematically in Fig. 3(a). As recently discovered, NiO is an

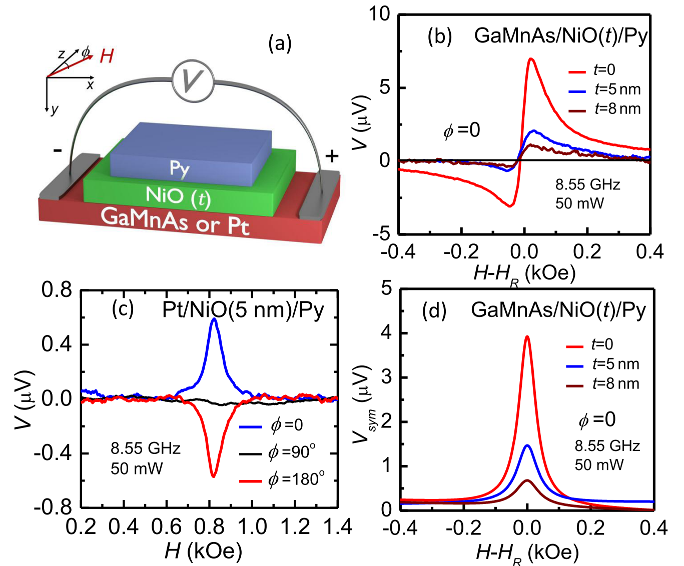

FIG. 3. (a) Sketch of the trilayer samples of (Ga,Mn)As/NiO (t)/Py (12 nm) and Pt (6 nm)/NiO (5 nm)/Py (12 nm). The GaAs and Si substrates are not shown (b) Voltage between the electrodes in (Ga,Mn)As (46 nm)/NiO (t)/Py for various NiO thicknesses, measured with FMR driven by a microwave field with frequency 8.55 GHz and power 50 mW, with the magnetic field at $\phi = 0$. (c) Voltage measured in the Pt/NiO/Py sample for three angles of the in-plane field with power 50 mW. (d) Symmetric components of the voltages for $\phi = 0$ in the three (Ga,Mn)As (46 nm)/NiO (t)/Py samples obtained with the least square fitting of Eq. (4) to the line shapes in (b).

insulating room temperature antiferromagnet that blocks the flow of charge current but transports spin currents [47–53]. Thus, one can study the spin-to-charge current conversion in (Ga,Mn)As, avoiding the superposition of the voltages due to ISHE in (Ga,Mn)As with the MCP effect in Py. In order to compare the data obtained in (Ga,Mn)As with the ones in a well-characterized normal nonmagnetic metal, we have also made a similar trilayer structure with a 6 nm thick Pt film sputter deposited on a Si(0.5 mm)/SiO(300 nm) substrate. Resistance measurements showed that the (Ga,Mn)As and Py layers were electrically isolated. The measured resistance between the electrodes is $R_N = 137\ \Omega$ in the Pt sample and $R_S = 2.4\ {\rm k}\Omega$ in the (Ga,Mn)As sample. This value is larger than in the sample of Fig. 2 because, here, the (Ga,Mn)As layer does not have the shunt effect of the Py layer.

Figure 3(b) shows the voltage measured in (Ga,Mn)As (46 nm)/NiO (t)/Py (12 nm) with NiO thicknesses of $t = 0$, 5, 8 nm, the same microwave frequency as in Fig. 2(c) and power of 50 mW. With the insertion of the NiO layer, the amplitudes decrease due to the decay of the spin current, and the line shapes become a little more symmetrical. The small antisymmetric components are attributed [7,23,39] to the anomalous Hall effect in (Ga,Mn)As produced by the dipolar coupling of the precessing magnetization in Py with the Mn spins in the S layer. Least square fits of Eq. (4) to the line shapes in Fig. 3(b) with superpositions of $L(H - H_R)$ and $D(H - H_R)$ functions yield the Lorentzian lines shown in Fig. 3(d). As expected, the peak amplitude of the voltage

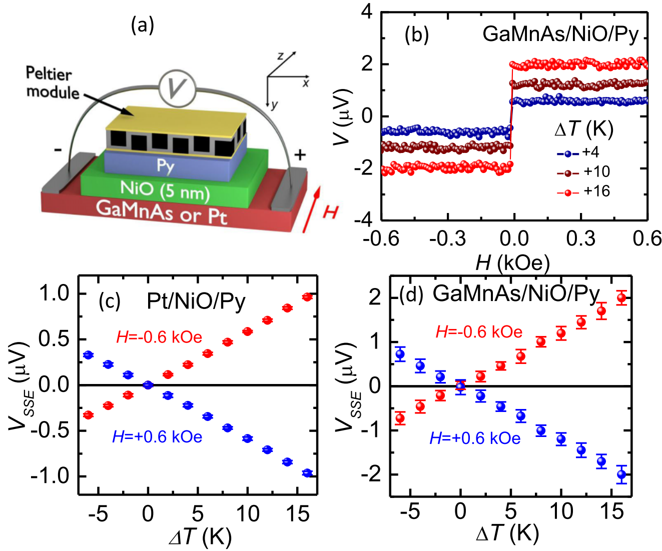

FIG. 4. (a) Schematic illustration of the sample used to measure the voltage generated in the (Ga,Mn)As (46 nm) or Pt (6 nm) layer produced by the ISHE conversion of the spin current generated by the LSSE in metallic Py. (b) Variation of the dc ISHE voltage V created by the SSE with the magnetic field intensity for three values of ΔT: $+4$, $+10$, and $+16$ K. (c) Variation of the voltage with temperature difference ΔT between the two sides of the Pt/NiO/Py sample. ΔT positive corresponds to the temperature larger at the Py layer. (d) Variation of V with ΔT measured in the (Ga,Mn)As/NiO/Py sample.

Lorentzian line decreases with increasing NiO thickness. Figure 3(c) shows the measured spin-pumping-ISHE voltages in the Pt (6 nm)/NiO (5 nm)/Py (12 nm) sample, for the same microwave power as in Fig. 3(d), exhibiting the expected field angle dependence. This result will be used as a reference to obtain the parameters for (Ga,Mn)As. The peak voltage in the (Ga,Mn)As/NiO(5 nm)/Py sample is 1.47 μV, while in Pt/NiO(5 nm)/Py, it is 0.58 μV, a ratio of 2.53. We note that, in the SPE, the spin current generated by the precessing magnetization in the Py layer flows in the $+y$ direction. Since for $\phi = 0$ the polarization is in the $+z$ direction, a charge current $\vec{J}_C = \theta_{SH}\, \vec{J}_S \times \hat{\sigma}$ in the $+x$ direction implies a positive spin Hall angle θ_{SH}. Hence, the positive signs of the voltages in Figs. 3(c) and 3(d) show that $\theta_{SH} > 0$ for both Pt and (Ga,Mn)As.

IV. SSE EXPERIMENTS

In order to confirm the spin-to-charge current conversion in (Ga,Mn)As by the ISHE, we have used another process to generate spin currents that does not have the subtleties of the line shapes of the spin-pumping voltages, namely the SSE. We have used the same samples of Fig. 2 with the schematic arrangement shown in Fig. 4(a). A commercial Peltier module, of width 1 mm, is used to heat or cool the side of the Py layer, while the substrate is maintained in thermal contact with a copper block at room temperature. The temperature difference ΔT across the sample is calibrated as a function of the current in the Peltier module by means of a differential thermocouple, with one junction attached to a thin copper strip placed between the Peltier module and the sample structure and the other between the sample and the copper block. After calibration, the thin copper strip and the thermocouple were removed so as not to interfere in the SPE and SSE measurements.

The temperature gradient across the Py layer generates a spin current by the SSE [54–58] that is injected into the NiO layer and is transported to the (Ga,Mn)As or Pt layer. Since the NiO layer provides electrical isolation of the Py layer, one can effectively measure the SSE spin current generated in the longitudinal configuration [59] without the contamination from the Nernst effect. Figure 4(b) shows the magnetic field dependence of the ISHE voltage in the (Ga,Mn)As layer produced by the spin current due to the SSE in the Py layer and transported by the NiO layer, for three values of the temperature difference ΔT across the sample structure: $+4$, $+10$, and $+16$ K (the $+$ sign means the Py side is warmer than the substrate). The data are qualitatively similar to the results obtained with the insulating ferrimagnet yttrium iron garnet (YIG), a standard material used in studies of the longitudinal SSE (LSSE) [55–61]. The change in the voltage sign with the field reversal is due to the change in the sign of the spin polarization. Figure 4(d) shows the measured variation of the voltage plateau V_{SSE} with the temperature difference ΔT for applied fields of $H = \pm 0.6$ kOe. The linear dependence of V_{SSE} on ΔT shows that the spin current generated by the LSSE in Py can be written as $J_S = -C_s \nabla T$, where ∇T is the temperature gradient across the Py layer and C_S is a spin Seebeck coefficient that depends on material parameters, similar to YIG/Pt [60,61]. For comparison, we have done measurements of V_{SSE} with ΔT in the Pt/NiO/Py sample, for $H = \pm 0.6$ kOe, as shown in Fig. 4(c). For $\Delta T = 16$ K, the V_{SSE} measured in the (Ga,Mn)As/NiO/Py sample is 2.0 μV, while in the Pt/NiO/Py sample, it is 0.95 μV, a ratio of 2.1.

V. DISCUSSION

With the insertion of a thin NiO layer between the Py and the (Ga,Mn)As layers, we have been able to do spin-pumping experiments without the contamination of the MCP effect and spin Seebeck experiments free from the anomalous Nernst effect. Both experiments show unequivocally that the spin current reaching the (Ga,Mn)As layer is partially converted into a charge current by the ISHE. From the experimental results presented, we can obtain the value of the spin Hall angle of $Ga_{0.95}Mn_{0.05}As$ at room temperature. First, it is necessary to consider the effect of the NiO layer. As shown in Ref. [53], the spin current density $J_S(0)$ injected in the Py/NiO interface is transported through the NiO layer (thickness t) by the diffusion of anti-FM magnons and reaches the interface at $y = t$ with a value proportional to $J_S(0)$, given by $J_S(t) = F_t\, J_S(0)$, where

$$F_t = c\,[\sinh(t/l_m) + c\,\cosh(t/l_m)]^{-1}, \quad (5)$$

where $c = g_{2\text{eff}}^{\uparrow\downarrow} b\, l_m / D_m$ is a dimensionless parameter proportional to the spin-mixing conductance of the interface at $y = t$, D_m and l_m are the diffusion constant and length of the magnon accumulation in NiO, and b is a factor involving integrations over the Brillouin zone. Since the broadening of the FMR line of Py in (Ga,Mn)As/NiO/Py due to the spin-pumping damping is very similar to that in Pt/NiO/Py, we can consider that their spin-mixing conductances are similar, and so are the factors F_t. Thus, regardless of the value of F_t, the ratio of the voltages

measured in the two systems, either with SPE or SSE, is, from Eq. (2)

$$\frac{V_S}{V_N} = \frac{R_S\,\lambda_S\,\theta_{\mathrm{SH}-S}\tanh(t_S/2\lambda_S)}{R_N\,\lambda_N\,\theta_{\mathrm{SH}-N}\tanh(t_N/2\lambda_N)}, \qquad (6)$$

where the subscripts S and N refer, respectively, to (Ga,Mn)As and Pt. Since the parameters for the reference material, Pt, are known, we can determine the spin Hall angle of (Ga,Mn)As, provided its spin diffusion length is known. By measuring the ratio of the spin-pumping voltages in two samples of (Ga,Mn)As (t_S)/NiO (5 nm)/Py (12 nm) with different thicknesses (46 and 92 nm) and using the relation $V_{S1}/V_{S2} = R_{S1}\tanh(t_{S1}/2\lambda_S)/R_{S2}\tanh(t_{S2}/2\lambda_S)$, we determined that $\lambda_S \approx 55$ nm. Using this value, the measured resistances $R_S = 2.4\,\mathrm{k}\Omega$ and $R_N = 137\,\Omega$, $\lambda_N = 3.7$ nm for Pt [10], and using for the ratio of the voltages in Eq. (6) an average of the values measured with SPE and SSE, $V_S/V_N = 2.3$, we can obtain the ratio between the spin Hall angles for $Ga_{0.95}Mn_{0.05}As$ and Pt. Considering that the latter, measured by several authors, is in the range $\theta_{\mathrm{SH}-N} = 0.04-0.10$ [3–10], we obtain for $Ga_{0.95}Mn_{0.05}As$ at room temperature $\theta_{\mathrm{SH}-S} = (1.5 \pm 0.5)\times 10^{-3}$. This value is two to three times smaller than the one measured in (Ga,Mn)As/Py, which shows that the MCP in Py [46] has a significant contribution to the voltage and cannot be overlooked.

The spin Hall angle for $Ga_{0.95}Mn_{0.05}As$ obtained in this paper is one order of magnitude larger than the values reported for p-Si [24] and for n-Ge [28]. In regard to other III-V semiconductors, Ref. [23] reports microwave spin-pumping measurements in Py/p-GaAs at room temperature. Although the authors of Ref. [23] do not explicitly calculate a value for the spin Hall angle in p-GaAs from the data, we note that, with microwave driving power of 200 mW, the SPE peak voltage in Ref. [23] is 300 nV, while we obtain with microwave power of 126 mW a symmetric peak voltage in (Ga,Mn)As/Py of 9 μV, as shown in Fig. 2(f). Note also that Ref. [39] reports spin-pumping measurements in (Ga,Mn)As/p-GaAs at low temperatures, where (Ga,Mn)As is in the FM phase. From the measured voltage, they obtain a value for the spin Hall angle in p-GaAs that is larger than ours for $Ga_{0.95}Mn_{0.05}As$. However, they did not consider the sizeable contribution to the voltage in p-GaAs arising from MCP in (Ga,Mn)As, an effect discovered later [40], so that their value is probably overestimated. It is not surprising that (Ga,Mn)As has a larger SHE than GaAs. As discussed in detail in Refs. [36,62], the strong spin-orbit coupling in the carrier bands and the exchange coupling of carrier spins with the dilute Mn local moments combine with the broken space-inversion symmetry in the host zinc-blende lattice to enhance the spin-orbit coupling of the spin carriers (Ga,Mn)As relative to GaAs.

In summary, we have demonstrated the spin-to-charge current conversion in the semiconductor of $Ga_{0.95}Mn_{0.05}As$ at room temperature by means of the ISHE. The spin currents were generated in a thin layer of Py by two different processes: SPE and SSE. In the first, we have used microwave-driven FMR of the Py film to generate a spin current that is injected into the (Ga,Mn)As film either in direct contact with Py or through a thin layer of insulating anti-FM NiO. In the second, we have used the SSE in the longitudinal configuration in Py with no contamination by the Nernst effect made possible with the use of a thin NiO layer between the Py and (Ga,Mn)As layers. The results of the two measurements are consistent with each other, and from them, we obtain a spin Hall angle for (Ga,Mn)As at room temperature of $\theta_{\mathrm{SH}} = (1.5 \pm 0.5)\times 10^{-3}$, which is one order of magnitude larger than the values reported for p-Si and for n-Ge. This result is significant for possible device applications with the integration of spintronics with semiconductor electronics.

ACKNOWLEDGMENTS

This research was supported in Brazil by Conselho Nacional de Desenvolvimento Científico e Tecnológico (CNPq), Coordenação de Aperfeiçoamento de Pessoal de Nível Superior (CAPES), Financiadora de Estudos e Projetos (FINEP), Fundação de Amparo à Pesquisa do Estado de Minas Gerais (FAPEMIG), and Fundação de Amparo à Ciência e Tecnologia do Estado de Pernambuco (FACEPE), and in Chile by Fondo Nacional de Desarrollo Científico y Tecnológico (FONDECYT) Grant No. 1170723.

[1] M. I. D'yakonov and V. I. Perel', JETP Lett. **13**, 467 (1971).
[2] J. E. Hirsch, Phys. Rev. Lett. **83**, 1834 (1999).
[3] A. Hoffmann, IEEE Trans. Mag. **49**, 5172 (2013).
[4] S. Maekawa, H. A. Adachi, K. Uchida, J. Ieda, and E. Saitoh, J. Phys. Soc. Jpn. **82**, 102002 (2013).
[5] J. Sinova, S. O. Valenzuela, J. Wunderlich, C. H. Back, and T. Jungwirth, Rev. Mod. Phys. **87**, 1213 (2015).
[6] A. Azevedo, L. H. Vilela-Leão, R. L. Rodríguez-Suárez, A. B. Oliveira, and S. M. Rezende, J. Appl. Phys. **97**, 10C715 (2005).
[7] E. Saitoh, M. Ueda, H. Miyajima, and G. Tatara, Appl. Phys. Lett. **88**, 182509 (2006).
[8] O. Mosendz, J. E. Pearson, F. Y. Fradin, G. E. W. Bauer, S. D. Bader, and A. Hoffmann, Phys. Rev. Lett. **104**, 046601 (2010).
[9] C. W. Sandweg, Y. Kajiwara, K. Ando, E. Saitoh, and B. Hillebrands, Appl. Phys. Lett. **97**, 252504 (2010).
[10] A. Azevedo, L. H. Vilela-Leão, R. L. Rodríguez-Suárez, A. F. Lacerda Santos, and S. M. Rezende, Phys. Rev. B **83**, 144402 (2011).
[11] L. H. Vilela-Leão, C. Salvador, A. Azevedo, and S. M. Rezende, Appl. Phys. Lett. **99**, 102505 (2011).
[12] L. Liu, C.-F. Pai, Y. Li, H. W. Tseng, D. C. Ralph, and R. A. Buhrman, Science **336**, 555 (2012).
[13] C. Hahn, G. de Loubens, O. Klein, M. Viret, V. V. Naletov, and J. Ben Youssef, Phys. Rev. B **87**, 174417 (2013).
[14] M. Weiler, M. Althammer, M. Schreier, J. Lotze, M. Pernpeintner, S. Meyer, H. Huebl, R. Gross, A. Kamra, J. Xiao, Y.-T. Chen, H. Jiao, G. E. W. Bauer, and S. T. B. Goennenwein, Phys. Rev. Lett. **111**, 176601 (2013).
[15] V. Castel, N. Vlietstra, B. J. van Wees, and J. Ben Youssef, Phys. Rev. B **90**, 214434 (2014).

[16] P. Hyde, L. Bai, D. M. J. Kumar, B. W. Southern, C.-M. Hu, S. Y. Huang, B. F. Miao, and C. L. Chien, Phys. Rev. B **89**, 180404(R) (2014).
[17] D. Weil, M. Obstbaum, M. Ribow, C. H. Back, and G. Woltersdorf, Nat. Commun. **5**, 3768 (2014).
[18] J. B. S. Mendes, R. O. Cunha, O. Alves Santos, P. R. T. Ribeiro, F. L. A. Machado, R. L. Rodríguez-Suárez, A. Azevedo, and S. M. Rezende, Phys. Rev. B **89**, 140406(R) (2014).
[19] W. Zhang, M. B. Jungfleisch, W. Jiang, J. E. Pearson, A. Hoffmann, F. Freimuth, and Y. Mokrousov, Phys. Rev. Lett. **113**, 196602 (2014).
[20] L. Bai, M. Harder, Y. P. Chen, X. Fan, J. Q. Xiao, and C.-M. Hu, Phys. Rev. Lett. **114**, 227201 (2015).
[21] C. Du, H. Wang, P. Chris Hammel, and F. Yang, J. Appl. Phys. **117**, 172603 (2015).
[22] Y. K. Kato, R. C. Myers, A. C. Gossard, and D. D. Awschalom, Science **306**, 1910 (2004).
[23] K. Ando, S. Takahashi, J. Ieda, H. Kurebayashi, T. Trypiniotis, C. H. W. Barnes, S. Maekawa, and E. Saitoh, Nat. Mater. **10**, 655 (2011).
[24] K. Ando and E. Saitoh, Nat. Commun. **3**, 629 (2012).
[25] E. Shikoh, K. Ando, K. Kubo, E. Saitoh, T. Shinjo, and M. Shiraishi, Phys. Rev. Lett. **110**, 127201 (2013).
[26] J.-C. Rojas-Sánchez, M. Cubukcu, A. Jain, C. Vergnaud, C. Portemont, C. Ducruet, A. Barski, A. Marty, L. Vila, J.-P. Attané, E. Augendre, G. Desfonds, S. Gambarelli, H. Jaffrès, J.-M. George, and M. Jamet, Phys. Rev. B **88**, 064403 (2013).
[27] S. Dushenko, M. Koike, Y. Ando, T. Shinjo, M. Myronov, and M. Shiraishi, Phys. Rev. Lett. **114**, 196602 (2015).
[28] F. Bottegoni, C. Zucchetti, S. Dal Conte, J. Frigerio, E. Carpene, C. Vergnaud, M. Jamet, G. Isella, F. Ciccacci, G. Cerullo, and M. Finazzi, Phys. Rev. Lett. **118**, 167402 (2017).
[29] H. Ohno, A. Shen, F. Matsukura, A. Oiwa, A. Endo, S. Katsumoto, and Y. Iye, Appl. Phys. Lett. **69**, 363 (1996).
[30] H. Ohno, Science **281**, 951 (1998).
[31] X. Liu and J. K. Furdyna, J. Phys.: Condens. Matter **18**, R245 (2006).
[32] D. Chiba, M. Sawicki, Y. Nishitani, Y. Nakatani, F. Matsukura, and H. Ohno, Nature **455**, 515 (2008).
[33] T. Jungwirth, J. Sinova, J. Masek, J. Kucera, and A. H. MacDonald, Rev. Mod. Phys. **78**, 809 (2006).
[34] Kh. Khazen, H. J. von Bardeleben, M. Cubukcu, J. L. Cantin, V. Novak, K. Olejnik, M. Cukr, L. Thevenard, and A. Lemaître, Phys. Rev. B **78**, 195210 (2008).
[35] T. Dietl and H. Ohno, Rev. Mod. Phys. **86**, 187 (2014).
[36] T. Jungwirth, J. Wunderlich, V. Novák, K. Olejník, B. L. Gallagher, R. P. Campion, K. W. Edmonds, A. W. Rushforth, A. J. Ferguson, and P. Němec, Rev. Mod. Phys. **86**, 855 (2014).
[37] H. Nakayama, L. Chen, H. W. Chang, H. Ohno, and F. Matsukura, Appl. Phys. Lett. **106**, 222405 (2015).
[38] C. M. Jaworski, J. Yang, S. Mack, D. D. Awschalom, J. P. Heremans, and R. C. Myers, Nat. Mater. **9**, 898 (2010).
[39] L. Chen, F. Matsukura, and H. Ohno, Nat. Commun. **4**, 2055 (2013).
[40] C. Ciccarelli, K. M. D. Hals, A. Irvine, V. Novak, Y. Tserkovnyak, H. Kurebayashi, A. Brataas, and A. Ferguson, Nat. Nanotechnol. **10**, 50 (2014).
[41] E. H. C. P. Sinnecker, G. M. Penello, T. G. Rappoport, M. M. Sant'Anna, D. E. R. Souza, M. P. Pires, J. K. Furdyna, and X. Liu, Phys. Rev. B **81**, 245203 (2010).
[42] H. Ohno, J. Magn. Magn. Mater. **200**, 110 (1999).
[43] Y. Tserkovnyak, A. Brataas, and G. E. W. Bauer, Phys. Rev. B **66**, 224403 (2002).
[44] Y. Tserkovnyak, A. Brataas, G. E. W. Bauer, and B. I. Halperin, Rev. Mod. Phys. **77**, 1375 (2005).
[45] S. M. Rezende, R. L. Rodríguez-Suárez, and A. Azevedo, Phys. Rev. B **88**, 014404 (2013).
[46] A. Azevedo, R. O. Cunha, F. Estrada, O. Alves Santos, J. B. S. Mendes, L. H. Vilela-Leão, R. L. Rodríguez-Suárez, and S. M. Rezende, Phys. Rev. B **92**, 024402 (2015).
[47] H. Wang, C. Du, P. C. Hammel, and F. Yang, Phys. Rev. Lett. **113**, 097202 (2014).
[48] C. Hahn, G. de Loubens, V. V. Naletov, J. Ben Youssef, O. Klein, and M. Viret, Europhys. Lett. **108**, 57005 (2014).
[49] H. Wang, C. Du, P. C. Hammel, and F. Yang, Phys. Rev. B **91**, 220410(R) (2015).
[50] T. Moriyama, S. Takei, M. Nagata, Y. Yoshimura, N. Matsuzaki, T. Terashima, Y. Tserkovnyak, and T. Ono, Appl. Phys. Lett. **106**, 162406 (2015).
[51] W. Lin, K. Chen, S. Zhang, and C. L. Chien, Phys. Rev. Lett. **116**, 186601 (2016).
[52] A. Prakash, J. Brangham, F. Yang, and J. P. Heremans, Phys. Rev. B **94**, 014427 (2016).
[53] S. M. Rezende, R. L. Rodríguez-Suárez, and A. Azevedo, Phys. Rev. B **93**, 054412 (2016).
[54] K. Uchida, S. Takahashi, K. Harii, J. Ieda, W. Koshibae, K. Ando, S. Maekawa, and E. Saitoh, Nature **455**, 778 (2008).
[55] G. E. W. Bauer, E. Saitoh, and B. J. van Wees, Nat. Mater. **11**, 391 (2012).
[56] H. Adachi, K. Uchida, E. Saitoh, and S. Maekawa, Rep. Prog. Phys. **76**, 036501 (2013).
[57] S. R. Boona, R. C. Myers, and J. P. Heremans, Energy Environ. Sci. **7**, 885 (2014).
[58] K. Uchida, H. Adachi, T. Kikkawa, A. Kirihara, M. Ishida, S. Yorozu, S. Maekawa, and E. Saitoh, Proc. IEEE **104**, 1946 (2016).
[59] K. Uchida, H. Adachi, T. Ota, H. Nakayama, S. Maekawa, and E. Saitoh, Appl. Phys. Lett. **97**, 172505 (2010).
[60] S. M. Rezende, R. L. Rodríguez-Suárez, R. O. Cunha, A. R. Rodrigues, F. L. A. Machado, G. A. Fonseca Guerra, J. C. Lopez Ortiz, and A. Azevedo, Phys. Rev. B **89**, 014416 (2014).
[61] S. M. Rezende, R. L. Rodríguez-Suárez, J. C. López Ortiz, and A. Azevedo, J. Magn. Magn. Mater. **400**, 171 (2016).
[62] A. Manchon and S. Zhang, Phys. Rev. B **78**, 212405 (2008).